Astronomy & Astrophysics manuscript no. accepted
January 20, 2013

On the driver of relativistic effects strength in Seyfert galaxies

M. Guainazzi[1], S. Bianchi[2,3], I. de la Calle Pérez[1], M. Dovčiak[4], A.L.Longinotti[5]

[1]European Space Astronomy Centre of ESA P.O.Box 78, Villanueva de la Cañada, E-28691 Madrid, Spain
e-mail: Matteo.Guainazzi@sciops.esa.int
[2]Dipartimento di Fisica, Università degli Studi Roma Tre, via della Vasca Navale 84, I-00146 Roma, Italy
[3]INAF-Osservatorio Astronomico di Brera, Via E.Bianchi 46, I-23807, Merate, Italy
[4]Astronomical Institute, Academy of Sciences, Boční II, 14131 Prague, Czech Republic
[5]MIT Kavli Institute for Astrophysics and Space Research, 77 Massachusetts Avenue, NE80-6011, Cambridge, MA, 02139

Received ; accepted

ABSTRACT

Context. Spectroscopy of X-ray emission lines emitted in accretion discs around supermassive black holes is one of the most powerful probes of the accretion flow physics and geometry, while also providing in principle observational constraints on the black hole spin. Previous studies have suggested that relativistically broadened line profiles are fairly common in nearby unobscured Seyfert galaxies. Their strength, as parametrised by the Equivalent Width (EW) against the total underlying continuum, spans a range of almost two orders of magnitude.

Aims. We aim at determining the ultimate physical driver of the strength of this relativistic reprocessing feature.

Methods. We first extend the hard X-ray flux-limited sample of Seyfert galaxies studied so far (FERO, de la Calle Pérez et al. 2010) to obscured objects up to a column density N_H=6 × 10^{23} cm^{-2}. We verify that none of the line properties depends on the AGN optical classification, as expected from the Seyfert unification scenarios. There is also no correlation between the accretion disc inclination, as derived from formal fits of the line profiles, and the optical type or host galaxy aspect angle, suggesting that the innermost regions of the accretion disc and the host galaxy plane are not aligned. We use this extended sample to study the EW dependency on various observables, and compare it with the predictions of Monte-Carlo accretion disc reprocessing simulations (George & Fabian 1991).

Results. The behaviour of the EW as a function of disc inclination, shape of the intrinsic power-law nuclear continuum, or iron abundance does not agree with the simulation predictions. Data are not sensitive enough to the detailed ionisation state of the line-emitting disc. However, the lack of dependency of the line EW on either the luminosity or the rest-frame centroid energy rules out that disc ionisation plays an important role on the EW dynamical range in Seyferts.

Conclusions. The dynamical range of the relativistically broadened K_α iron line EW in nearby Seyferts appears to be mainly determined by the properties of the innermost accretion flow. We discuss several mechanisms (disc ionisation, disc truncation, aberration due to a mildly relativistic outflowing corona) which can explain this. We stress that the above results as such do not represent either a falsification or a proof the relativistically blurring scenario. Observational data are still not in contradiction with scenarios invoking different mechanisms for the spectral complexity around the iron line, most notably the "partial covering" absorption scenario.

Key words. Accretion discs - Relativistic processes - Galaxies:nuclei - Galaxies:Seyfert - X-ray:galaxies

1. X-ray spectroscopic evidence for relativistic accretion flow in AGN

Accretion discs feeding black holes are predicted to dissipate most of their energy in the innermost few Schwarzschild radii (Agol & Krolik 2000, Krolik & Hawley 2002). In these regions, the space-time distortion affects significantly the photon path through general and special relativity effects (Fabian et al. 2000, Reynolds & Novak 2003). Monochromatic lines emitted in relativistic discs are expected to suffer significant profile distortions (Fabian et al. 1989, Laor 1991). The properties of the profiles as seen at infinity depend on a number of parameters related to the accretion flow (size and ionisation state of the disc photosphere), its orientation with respect to the line of sight, the shape of the illuminating ionising continuum (Matt et al. 1992, Życki et al. 1994, Nayakshin et al. 2000, Ross & Fabian 2005) and the metal abundances. The profile in principle probes the physical and geometrical properties of the accretion flow on spatial scales inaccessible by any other conceivable experiments in the electromagnetic domain.

That's the reason why great excitement followed the first detection of a broadened and skewed profile of the iron K_α fluorescent iron line by ASCA in MCG-6-30-15, a nearby X-ray bright Seyfert 1 galaxy (Tanaka et al. 1995). Broad iron lines were common in ASCA spectra of AGN (Nandra et al. 1997). With the launch of major X-ray observatories at the beginning of the century - *Chandra* and XMM-Newton - the hope arose to be able to accumulate large samples of broad lines, which may unveil experimental clues on the way matter accretes onto supermassive black holes, as well as allow us to study its dependence on the AGN and host galaxy properties. This hope has been only partly fulfilled. Although

Send offprint requests to: M.Guainazzi

there are plenty of measurements of broad iron K_α lines (Miller 2007) (as well as from other elements or iron transitions: Mason et al. 2003, Fabian et al. 2009), many of them have been challenged as non-unique solutions to the complexity of the AGN spectra (Reeves et al. 2004, Turner & Miller 2009, Miller & Turner 2010). The controversy is fierce. This controversy will *not* be the subject of this paper. We will assume in the following that relativistic broadening and skewing is the correct astrophysical scenario to interpret the observed line profiles. If this assumption turns out to be wrong, the conclusions of this paper will be, it goes without saying, wrong as well.

Recently studies of large AGN samples focusing on the properties of their relativistic lines have been published (Nandra et al. 2007, de la Calle Pérez et al. 2010). The main conclusions of these studies can be summarised as follows:

- relativistically broadened iron K_α fluorescent lines are present in 35–45% of bright nearby ($z \leq 0.01$) Seyfert galaxies. However, taking properly into account the sensitivity limits of the available observations, the presence of a broad line with EW >30 eV cannot be excluded in 87% of the parent population. At even lower EW values one hits the parameter space where systematic calibration uncertainties dominate
- the line shape is consistent with it being emitted in a moderately relativistic accretion disc, as parametrised by the power-law index of the emissivity radial dependence, α ($\langle\alpha\rangle = 2.4 \pm 0.5$) once emission down to the innermost circular stable orbit is assumed. In a few cases, however, data require a significantly steeper law (notably MCG-6-30-15, Wilms et al. 2001, Fabian & Vaughan 2003; 1H0707-495, Fabian et al. 2009; IRAS13224+3803, Ponti et al. 2010). This has been interpreted as evidence in favour of extreme light bending affecting the line photon paths (Miniutti & Fabian 2004)
- the accretion disc inclination distribution, $\imath$, is peaked around $\simeq$30°. However, this could be primarily due to an observational bias against lines produced in highly inclined discs (Matt et al. 1992). Indeed, the measured disc inclination distribution is still consistent with an intrinsic random distribution (Nandra et al. 1997, Nandra et al. 2007, de la Calle Pérez et al. 2010).
- the line Equivalent Width (EW) spans a range of almost one order of magnitude ($\sim$30–300 eV). In a few cases, even larger EW have been measured (4U1344-60, Piconcelli et al. 2006; AXJ0447-0627, Della Ceca et al. 2005: H1413+117, Chartas et al. 2007; IRAS 1334+2438, Longinotti et al. 2003: MCG-02-14-009, Porquet 2006; Mkn 335, Longinotti et al. 2007; NGC 1365, Risaliti et al. 2009; PG1543+489, Vignali et al. 2008; RBS1423, Krumpe et al. 2007), again possibly indicative of reflection-dominated states induced by strong light bending (Miniutti & Fabian 2004)
- the line properties and intensities are independent of the black hole mass (as the theory postulates; Fabian et al. 1989, Matt et al. 1992), luminosity or accretion rate

A standard plane-parallel X-ray illuminated accretion disc covering a 2π solid angle should produce an EW$\sim$150 eV for a typical AGN X-ray spectral shape and solar abundances (George & Fabian 1991). The less-than-100% detection fraction, as well as this large variety of EW values need an explanation.

In this paper we aim at investigating the ultimate physical driver of the observed broad iron line strength. For this purpose we first extend the samples published so far, which included primarily X-ray unobscured AGN, to the whole Seyfert population up to column densities whose photoelectric cut-off does not hamper the measurement of the continuum underneath the line (Sect. 2). This allow us to investigate the correlation between the detection of a relativistically broadened iron line and AGN classification and host galaxy properties. Subsequently (Sect. 3) we perform a falsification test of the currently accepted paradigm that the main driver of the line EW is the solid angle covered by the disc at the X-ray source, possibly modified by General Relativity effects for the strongest lines. We discuss our results in Sect. 4.

2. The GREDOS sample

We extract the GREDOS (*General Relativity Effects Detected in Obscured Sources*) sample by correlating the 54 months 14-195 keV *Swift Palermo BAT Catalogue* (PBC; Cusumano et al. 2010) with the XMM-Newton observation log as of August 2010. The parent sample includes 754 AGN. The definition of the GREDOS sample is solely based on X-ray spectral properties. In order for a source to to belong to GREDOS, the column density measured from a simple power-law continuum fit of the XMM-Newton EPIC spectra in an optimal observation-dependent energy band has to be comprised between 5×10^{21} and 6×10^{23} cm^{-2}. Actually, only one of the GREDOS objects (1ES0241+622) has got a column density <10^{22} cm^{-2}. The algorithm to determine this "optimal energy band" will be explained in Sect. 2.1. Moreover, we have retained only sources with a BAT flux $\geq 4 \times 10^{-11}$ erg cm^{-2} s^{-1}. This value corresponds to the count rate threshold used by de la Calle Pérez et al. (2010) to define a flux-limited sub-sample (FERO *Finding Extreme Relativistic Objects*) of the RXTE All Sky Survey (Revnivtsev et al. 2004).

The aforementioned upper threshold on N_H (6×10^{23} cm^{-2}) has been chosen to ensure that the obscuring column density does not prevent the view of the primary emission at the energies of the iron emission features in any of the GREDOS objects.

The results on the GREDOS sample in this paper will be compared to and jointly discussed with a sample extracted from the flux-limited FERO sample (de la Calle Pérez et al. 2010). The latter comprises all the flux-limited FERO AGN (21 sources)[1]. whose X-ray spectrum is obscured by a "cold" photoelectric column density <5×10^{21} cm^{-2}. The FERO sub-sample so defined is therefore complementary to GREDOS. The FERO and GREDOS samples together can be used to test the invariance of the relativistically broadened features with optically

[1] Ark 120, Ark 564, ESO 198-G24, Fairall 9, H0557-385, IC 4329A, MCG-2-58-22, MCG-6-30-15, MCG+8-11-11, MR 2251-178, Mrk 110, Mrk 279, Mrk 509, Mrk 766, NGC 3516, NGC 3783, NGC 4051, NGC 5548, NGC 7314, NGC 7469, UGC 3973

Table 2. List of merged observations for GREDOS sources.

Source	Merged Obs.#
NGC 4151	0112310101 0112830201, 0112830501
NGC 526A	0150940101 0109130201
NGC 5506	0554170101, 0554170201
MCG-5-23-16	0112830301, 0302850201

defined spectral type which is predicted by the Seyfert unification scenarios.

The GREDOS sample comprises 13 objects (Tab. 1).[2] It is important to stress that GREDOS is neither a complete nor an unbiased sub-sample of PBC. XMM-Newton observed some of the GREDOS objects multiple times. We have at first separately analysed the individual time-averaged spectra with simple photoelectrically absorbed power-law models. Spectra corresponding to best-fit parameter values consistent within the statistical uncertainties were merged together. For each source we retained only the spectrum with the longest exposure time after this merging process. This is the same procedure followed with the FERO sources (de la Calle Pérez et al. 2010). In Tab. 2 we show the list of XMM-Newton Observations IDs which were merged together.

2.1. Data reduction and analysis

In this paper we discuss data taken with the EPIC cameras only: EPIC-pn (Strüder et al. 2001), and EPIC/MOS (Turner et al. 2001). Data were reduced using SASv10 (Gabriel et al. 2003), using the calibration files available in August 2010. Calibrated event lists were generated using the reduction meta-tasks `e[mp]proc`. Source spectra were extracted from circular extraction regions centred around the source X-ray centroid. The size of the source scientific products extraction region r_e, as well as the count rate thresholds C_t employed to reject intervals of high particle background were determined through an iterative process to maximise the net source spectra signal-to-noise ratio (see Tab. 1). To measure the particle-induced background we used the whole field-of-view, high-energy (MOS: $E > 10$ keV; pn: 10 keV $\leq E \leq$ 12 keV) light curve binned to Δt=10 s. Background spectra were extracted from off-axis circular regions on the same CCD as the source, and additionally at the same `RAWY` position in the EPIC-pn camera to ensure that the same charge transfer efficiency correction applies, as this correction depends on the distance from the readout node. Response files for each spectrum were generated using the SAS tasks `arfgen` and `rmfgen`.

Spectra were rebinned in order to ensure that: a) each background-subtracted spectral channel contains at least 50 counts; b) the instrumental intrinsic resolution is oversampled by a factor not larger than 3. These conditions ensure that we can use the χ^2 as a goodness-of-fit test in the forthcoming spectral analysis. Spectral fits were performed in the energy range [E_{soft},10.0 keV]. E_{soft} (see Tab. 1) was determined for each spectrum after visual inspection as the energy where excess emission above the extrapolation of the photoelectrically absorbed power-law emission starts to dominate. The rationale behind this choice is driven by the empirical evidence that this soft excess is associated to diffuse emission extended on scales as large as a few kiloparsecs, most likely due to gas associated to the Narrow and Extended Narrow Line Regions (Bianchi et al. 2006), with contribution by strong starburst emission in a few objects (Guainazzi et al. 2009). The modelling of this component is therefore fully decoupled from that of the the primary nuclear emission.

In this paper we quote statistical errors at the 90% confidence level for one interesting parameter unless otherwise specified. In order to calculate luminosities we use the following cosmological parameters: H_0=70 km s^{-1} Mpc^{-1}, Λ_0=0.73, Ω_M=0.27 (Bennett et al. 2003).

2.2. Spectral model definition

The main feature characterising X-ray spectra of obscured AGN is a soft X-ray photoelectric cut-off due to high column densities of obscuring gas (Awaki et al. 1991). We therefore first fit the GREDOS spectra with a simple baseline continuum constituted by a power-law modified by photoelectric absorption trough cold matter. However, moderate-resolution spectroscopy of nearby Seyfert galaxies unveils further spectral complexity, associated to reprocessing of the primary nuclear continuum (Pounds et al. 1990, Nandra & Pounds 1994, Turner et al. 1997). This evidence led us to add to the model continuum a Compton-reflection component (model `pexrav` in XSPEC; Magdziarz & Zdziarski 1995) as well as a number of Gaussian emission line profiles to account for K_α (with its Compton shoulder; Matt 2002) and K_β fluorescent lines from neutral iron (Turner et al. 1997), and for recombination lines from He- and H-like iron (Netzer et al. 1998, Bianchi & Matt 2002). This "non-relativistic" baseline model can be described as follows:

$$M(E) = e^{-\sigma_p(E)N_H} \times [A_1 E^{-\Gamma} + \Sigma_i N_i G_i(E_i) +$$

$$A_2 C_S(E)] + A_3 C_R(E, \Gamma)$$

where σ_p is the photoelectric cross-section, G_i are Gaussian profiles, C_S is the Compton shoulder, C_R is the Compton reflection continuum, and A_i and N_i are normalisation constants. We used the `ztbabs` implementation for the photoelectric absorption in XSPEC. In the baseline, as well as in all subsequent more complex models, we made the following assumptions:

– the photon index Γ of the power-law and of the Compton reflection continuum has been constrained to be the same
– the power-law is modified by a high-energy cut-off beyond the energy bandpass of the EPIC cameras. It have been held fixed to 150 keV (Risaliti 2002)
– the inclination of the Compton reflection component with respect to the line-of-sight has been held fixed to 45°. This parameter is degenerate with the relative normalisation between the Compton reflection and the primary continuum, therefore this assumption does not unnecessarily constraint the parameter space of other spectral parameters

[2] Two objects in GREDOS (MCG-5-23-16, NGC 526A) belong to the FERO flux-limited sample after de la Calle Pérez et al. (2010) due to the slightly different column density thresholds employed by them to define an object as "X-ray unobscured".

Table 1. The GREDOS sample.

Obs.#	NED Name	Type[a]	z	f_{BAT}[b]	E_{soft}[c]	r_e[d]	C_t[e]	T_{exp}[f]
0006220201	NGC4507	Sy2	0.012	146.0	3.0	60/ 67	0.35/ 0.5	42.0/ 33.2
0067540201	Mrk348	Sy2	0.015	112.0	2.5	60/ 40	1/ 2	26.4/ 22.5
0110930701	NGC4388	Sy2	0.008	203.0	3.0	68/ 32	0.5/ 1	11.5/ 7.3
0144230101	Mrk6	Sy1.5	0.019	43.7	1.0	85/ 37	0.35/ 0.5	36.0/ 31.3
0145670101	NGC2110	Sy2	0.008	215.0	1.5	81/ 35	0.35/ 0.5	34.0/ 34.8
0152940101	NGC5252	Sy2	0.022	60.1	2.0	67/ 38	0.35/0.35	41.0/ 33.3
0202860101	NGC7172	Sy2	0.009	119.0	1.5	77/ 38	1/ 2	44.6/ 40.0
0550450301	1ES0241+622	Sy1.2	0.045	51.0	1.0	70/ 40	1/ 35	15.2/ 12.1
0550451501	GRS1734-292	Sy1	0.021	103.0	1.0	112/ 38	1/ 0.5	17.2/ 13.5
Tab. 2	NGC5506	Sy2	0.006	196.0	2.0	50/ 50	0.35/0.35	61.0/117.8
Tab. 2	NGC4151	Sy1.5	0.003	376.0	2.2	38/ 39	0.35/ 0.5	87.5/ 71.9
Tab. 2	NGC526A	Sy1.9	0.019	42.6	1.2	89/ 38	0.35/ 0.5	53.7/ 45.4
Tab. 2	MCG-05-23-016	Sy2	0.008	166.0	1.8	40/ 47	0.35/ 0.5	118.4/104.8

[a]optical Seyfert type according to the Véron-Cetty & Véron catalogue (Véron-Cetty & Véron 2010)
[b]14–195 keV BAT flux (in units of 10^{-12} erg cm^{-2} s^{-1}) after Cusumano et al. (2010)
[c]low boundary of the energy interval where the spectral fit was performed
[d]size (in arc-seconds) of the source spectrum extraction region (MOS/pn)
[e]threshold (in counts per second) on the single-events, high-energy light curve to reject intervals of high particle background (MOS/pn)
[f]net exposure time in ks (MOS/pn) after data screening

– we have assumed solar abundances according to Anders & Grevesse (1989)
– the centroid energy of the Gaussian profiles has been held fixed to values as dictated by the atomic physics: 6.4 keV, 6.966 keV, 7.058 keV for Fe I K_α, Fe XXVI, and Fe I K_β, respectively. The intensity of the Fe I K_β has been constrained not to exceed 16% that of the K_α. For the Fe XXV transitions we have allowed the centroid energy to vary between 6.6364 and 6.7000 keV, corresponding to the forbidden and the resonant transitions, respectively
– the intrinsic width of the Gaussian profiles has been assumed to be the same for a given object, and consistent with the instrumental resolution
– following Matt (2002), the Compton shoulder was modelled with a rectangular box of width 50 eV and intensity constrained not to exceed 20% of the intensity of the corresponding K_α profile

Only after these additional components were included (and kept, if their inclusion improved the quality of the fit at a confidence level >90%; Lampton et al. 1976), we tried to fit any further spectral complexity with relativistically blurred disc components. For this scope, we have used models extracted from the `ky` suite (Dovčiak et al. 2004), based on a common ray-tracing subroutine aiming at describing the X-ray emission of black-hole accretion discs in the strong gravity regime. As any emission line should come accompanied by a relativistically blurred disc continuum, we have used a combination of the models `kyrline` and `pexrav` where the latter was convolved with a relativistic kernel `kyconv`. In both `kyrline` and `kyconv` the blurring effect depends on the following parameters: a) the black hole spin a (comprised between 0 and 0.9982 in dimensionless relativistic units); b) the inner (r_{in}) and outer (r_{out}) radius of an annular region on the disc where the line photons are emitted; c) the index α of the radial dependence of the emissivity per unit area, κ, in the local frame comoving with the disc: $\kappa(r) \propto r^{-\alpha}$; d) the "disc inclination" $\imath$, i.e. the angle between the normal to the disc plane and the line-of-sight; e) the rest frame energy (assumed monochromatic) of the photons emitted by the disc, E_c. Although the line normalisation in `kyrline` is expressed in units of photons cm^{-2} s^{-1} integrated over the whole profile, we will also use the line Equivalent Width (EW), i.e. the line intensity normalised to the underlying continuum at 6.4 keV, to ease comparison against theoretical predictions. Following the approach described in Guainazzi et al. (2010), we fixed the values of r_{in} and r_{out} to the innermost circular stable orbit (e.g. $r_{in} = 1.24 r_g$ for a maximally spinning black hole) and r_{out}=400r_g, respectively. Constraints on the black hole spin could not be derived for any of the GREDOS sources. We therefore assumed a maximally spinning black hole in all the subsequent fits.

For objects where this model did not provide an adequate fit we changed the obscuration law. We have tried the following additional prescriptions for the X-ray obscuration: a) two "cold" absorbing systems, one covering the primary and the relativistically broadened reprocessing components, and the other covering the whole model; b) a partial covering absorber covering solely the primary and the relativistically broadened reprocessing components; c) one ionised absorber, calculated according to a grid of Cloudy models (Ferland et al. 1998) as described in Bianchi et al. (2010); d) the combination of a "cold" and a "ionised" absorber.

For each source we have selected the model which yields the best reduced χ^2. We consider in the following a relativistic line as detected if the variation of χ^2 associated with the inclusion of the `kyrline` component in the spectral model is significant at the 5-σ level, to be consistent with the criterion adopted by de la Calle Pérez et al. 2010.

2.3. Spectral results

Tab. 3, and Tab. 4 of Appendix A summarise the results of our spectral fits on the GREDOS sample. At the adopted 5-σ confidence level, a broadened relativistic line is detected in only two sources. In both cases this detection was reported elsewhere: MCG-5-23-16 (Dewangan et al. 2003, Reeves et al. 2007, de la Calle Pérez et al. 2010), and

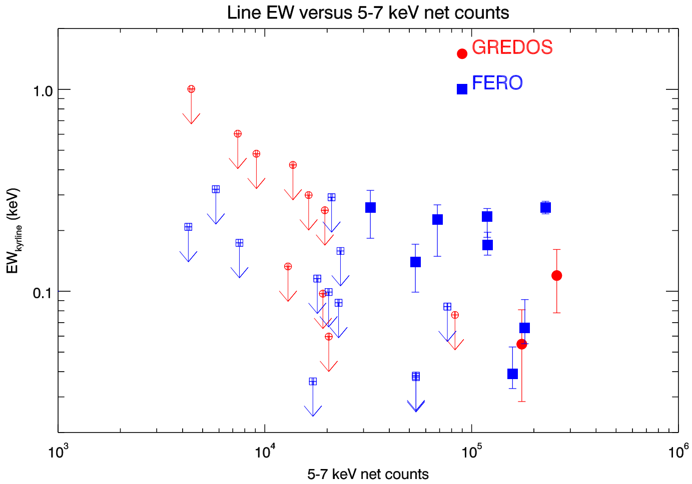

Fig. 1. Relativistic line EW as a function of the background-subtracted 5–7 keV counts in the GREDOS (*circles*) and FERO (*squared*) samples sources. *Empty symbols* indicate upper limits. The *lines* represent the sample sensitivity for three different values of inclination angle, assuming $\alpha = 2.5$: *dashed line*: 10°; *dot-dashed line*: 40°; *dot-dot-dashed line*: 80°.

NGC 5506 (Guainazzi et al. 2010). Our non-detections are also consistent with published reports: Mkn 6 (Schurch et al. 2006), NGC 4151 (Schurch et al. 2003), NGC 4388 (Beckmann et al. 2004), NGC 5252 (Dadina et al. 2010). The detection fraction in GREDOS ($\simeq$15%) is nominally lower then in samples of unobscured AGN. However, the GREDOS sample is incomplete. This prevents a statistically robust comparison of this number with less unbiased samples such as FERO. Moreover, most of the GREDOS sources are underexposed. In Fig. 1 the EW of the relativistic line is plotted against the background-subtracted counts in the 5–7 keV energy band. As already observed by other authors (Guainazzi et al. 2006, de la Calle Pérez et al. 2010), the detection is a strong function of the number of net source counts in the hard X-ray band. All broad line detections in the FERO and in the GREDOS samples correspond to objects with more then 30,000 net source counts in the 5–7 keV energy band. Only three sources in GREDOS satisfy this empirical criterion: MCG-5-23-16, NGC5506 (the two detections), and NGC 4151. Intriguingly enough, above 100,000 net counts one measures a 100% detection fraction.

At a lower confidence level (3σ) an additional broad line is detected in a GREDOS source: in NGC 4507, by contrast to Matt et al. 2004. Its parameters are: $\alpha \leq 1.7$, $\imath = 10\pm^{4\circ}_{8}$, $EW = 128\pm^{4}_{60}$ eV if $E_c \equiv 6.4$ keV. We will not include this measurement in the joint analysis of the FERO and GREDOS detections (see Sect. 2.4). The profiles of the iron lines in GREDOS are shown in Fig. 2. These line profiles are obtained from the data/model ratio against the best-fit once the relativistic line profile (`kyrline` component) is removed. In Fig. 3 we show the fractional contribution of the continuum as well as of the narrow-band emission features to the total best-fit model in the two GREDOS objects, where a broad line is detected at a confidence level $\geq 5\sigma$.

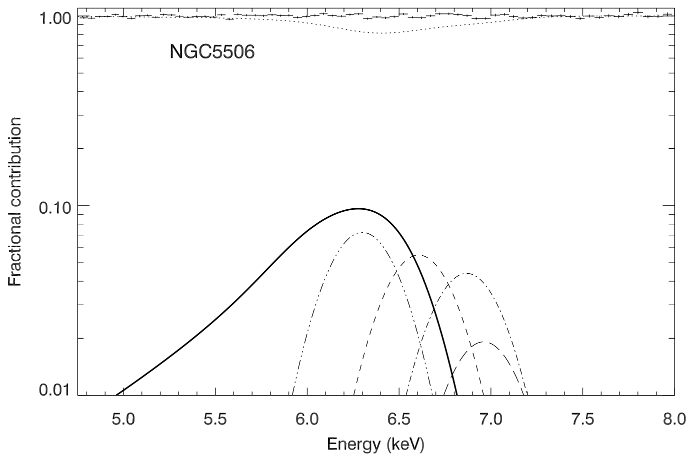

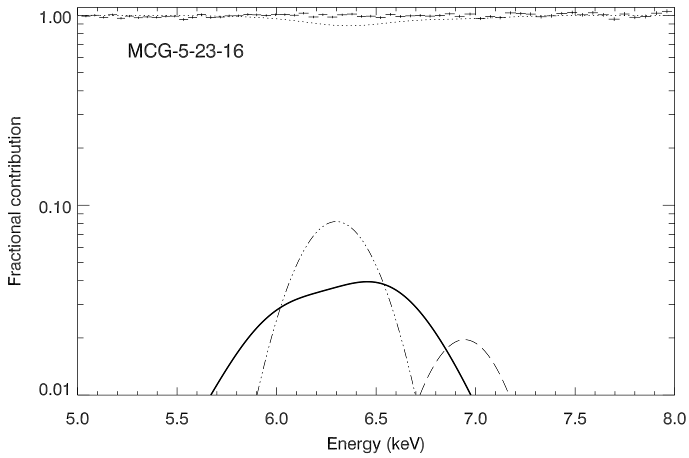

Fig. 3. Fractional contribution of the best-fit model components to the total best-fit model. *Dotted line*: continuum; *solid line*: relativistically broadened Fe; *dashed-multi-dotted line*: unresolved FeI K_α; *dashed line*: unresolved FeXXV recombination; *dashed-dotted line*: unresolved FeXXVI recombination; *dashed line*: unresolved FeI K_β line. All components have been smoothed with a Gaussian kernel (σ_{kernel}=150 eV) to reproduce the effect of the EPIC-pn intrinsic energy resolution. The *crosses* represents the data/model ratio against the best-fit model.

2.4. FERO+GREDOS detections

Hereafter we will consider the detections in the FERO and GREDOS samples jointly (cf. Sect.2 for the definition of the FERO sample in this paper). In this sample, 12 broad iron lines are detected at confidence level $\geq 5\sigma$ (cf. Tab. 2 in de la Calle Pérez et al. 2010, and Tab. 4 in this paper).

Once the FERO and GREDOS detections are considered jointly, neither the detection fraction, nor the line EW are dependent on the optical type (Fig. 4), despite a nominal trend for broad lines to be more common in "type 1" Seyferts. In this paper we use the optical type as defined in the Veron-Cetty & Veron (2010) catalogue. We use the optical classification to situate, at the best of our knowledge, the FERO+GREDOS sources in the framework of the standard Seyfert unification scenario as reviewed in, *e.g.*, Antonucci (1993). For this purpose, objects which ex-

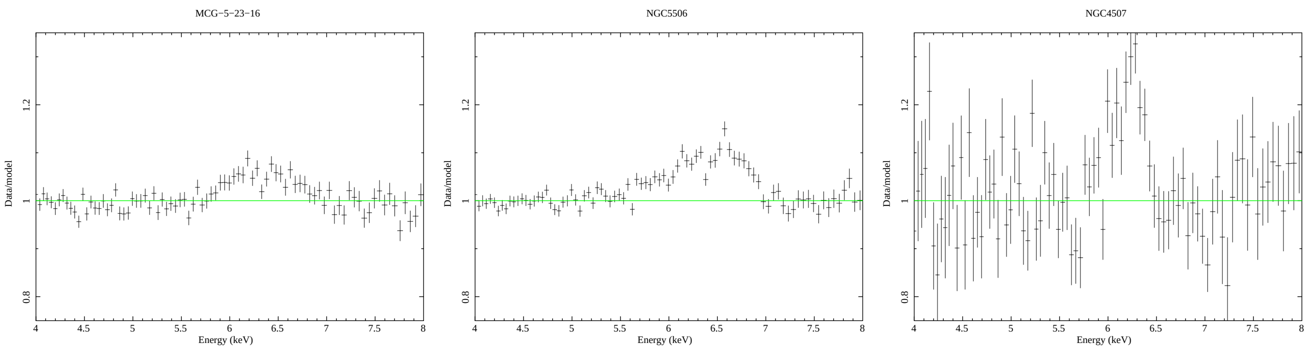

Fig. 2. Profiles of the relativistically broadened iron lines detected in the GREDOS sample. They represent data/model ratios once the `kyrline` component is removed from the best-fit model. The lines in MCG-5-23-16 and NGC 5506 are detected at a confidence level $\geq 5\sigma$ in the relativistically blurred line scenario. The line in NGC 4507 is detected at a confidence level $\simeq 3\sigma$ only.

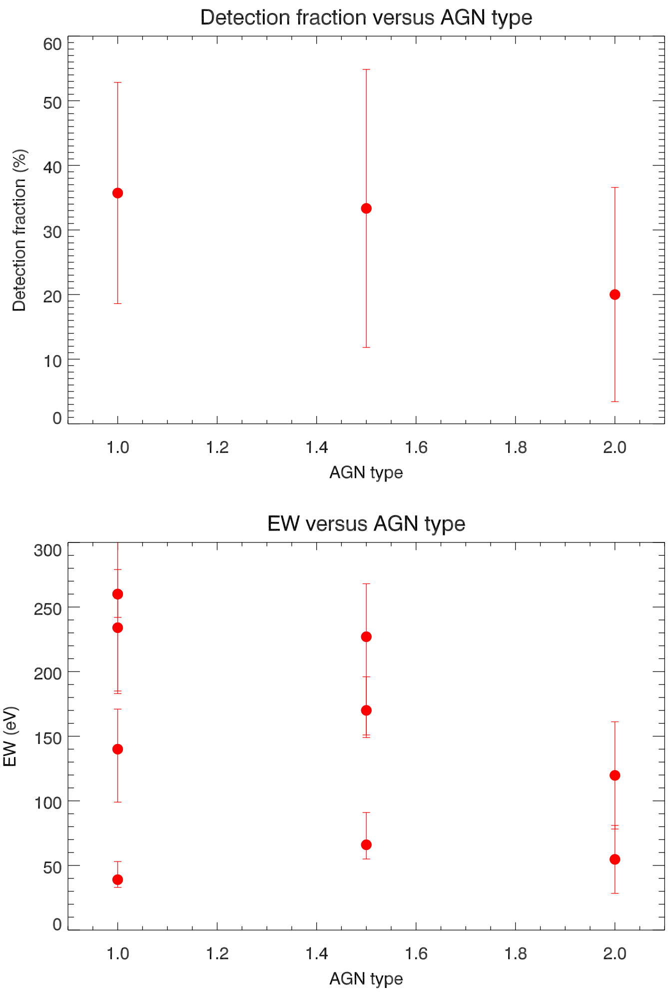

Fig. 4. Relativistic line detection fraction (*upper panel*) and EW (*lower panel*) as a function of optical type for the sources of joint FERO+GREDOS samples.

hibit broad polarised Balmer lines and/or weak IR broad lines, but whose optical spectrum is typical of obscured AGN are still considered "type 2"[3]. For sake of simplicity we include Veron type 1.9 objects into the "type 2" class, Veron type 1.2 objects and Narrow Line Seyfert galaxies[4] into the "type 1" class, hereafter.

Following the same approach as in, *e.g.*, Guainazzi et al. (2010) we use the α parameter in `kyrline` as a measurement of the importance of relativistic effects in shaping the profile of the iron K_α emission line. For the same value of the inner and outer radius of the line-emitting region being equal, higher α values indicate that line photons are emitted in regions closer to the accretion disc innermost stable orbit. For $\alpha \leq 2$ (*i.e.* when a large fraction of the accretion disc is responsible for the line production) the choice of the line-emitting region outer radius (which, we remind, is fixed to $400 r_g$ in our spectral models) may affect the best-fit values of other line parameters. This effect is discussed by Guainazzi et al. (2010) for the case of NGC 5506.

In the joint FERO and GREDOS detections one observes an apparent correlation between α and EW (Fig. 5). A fit to the data using an extension of the regression method on censored data originally described by Schmitt (1985) and Isobe et al. (1986) yields: $\alpha = (0.44 \pm 0.19) + (2.0 \pm 0.8) \times \log(EW)$, when EW is expressed in keV. The Spearmann rank coefficient on the same data yields a correlation probability of $99.7 \pm^{0.2}_{17.4}$%, where the nominal value is calculated using only bracketed measurements, and the error bars reflect the range of values that censored data could cover on the y-axis (only subject to the best-fit model parameter restriction: $\alpha \leq 6$). Taking into account the large uncertainties, the correlation is statistically marginal. In the same figure, we compare the measurements with the predictions of an axisymmetric lamppost model (Dovčiak et al. 2004), where a point-like source of X-ray radiation is located at variable heights along the black hole spin axis. We simulated EPIC-pn spectra according to this model, and fit them using the same baseline model as defined in Sect. 2.2. Moderately relativistic ($\alpha \lesssim 3$) lines can be explained in this framework if the accretion disc is seen in different objects under a wide range of different inclination angles and heights. Interestingly enough, it is impossible to get $\alpha > 3$ in this scenario. Recently, examples of extreme relativistic lines have been published, whose profiles are consistent with very steep ($\alpha \gtrsim 5$) specific emissivity radial dependencies (Wilms et al. 2001, Fabian et al. 2009, Ponti et al. 2010).

[3] MCG-5-23-16, Mkn 348, NGC 2110, NGC 4388, NGC 4507, NGC 5506, NGC 7314

[4] Mkn 110, Mkn 766, NGC 4051

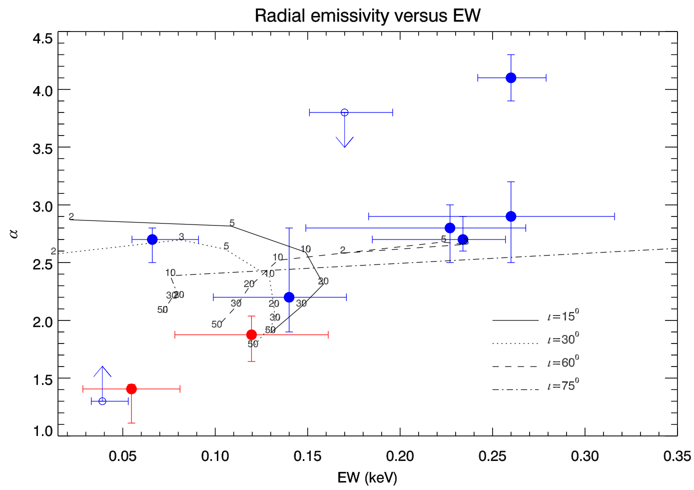

Fig. 5. α versus EW for the iron K_{α} relativistic lines detected in the FERO and GREDOS samples. *Empty symbols* indicate upper limits. The *lines* represent the predictions of a lamppost model for different values of the X-ray source height (*small numbers along the curves* in units of gravitational radii) and disc inclinations (*line styles*; cf. the inset label).

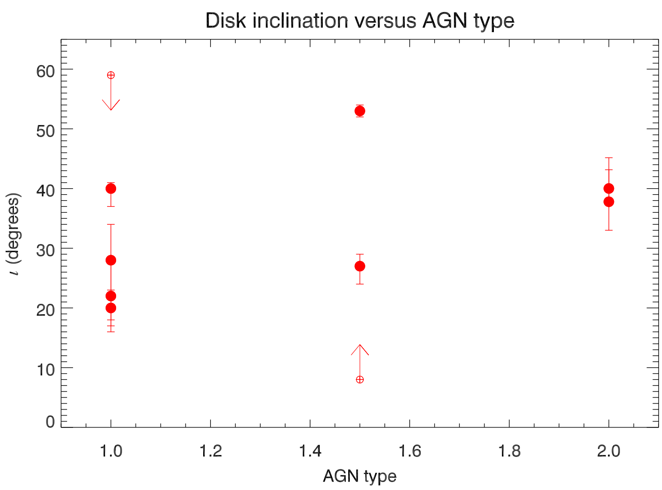

Fig. 6. Accretion disc inclination angle $\imath$ as a function of the optical type for the joint GREDOS and FERO control sample discussed in this paper.

The main driver for some of these results is the very smooth shape of the soft excess, implying extreme relativistic blurring of narrow-band spectral features imprinted by disc reflection on the soft X-ray ($E \lesssim 2$ keV) spectrum. As pointed out by, *e.g.*, Życki et al. (2010) steep profiles can be obtained only if the X-ray source is not located on the black hole spin axis, because they require the combination of dynamical Doppler shift and frame dragging within the black hole ergosphere.

There is no significant difference between the distribution of disc inclination angles between the GREDOS and the FERO sample sources, neither a dependency of the disc inclination angle on the optical spectral type (Fig. 6) or host galaxy inclination. Although the line detections in type 2 Seyfert correspond to $\imath \geq 38°$ (MCG-5-23-16, Reeves et al. 2007; NGC 5506, Guainazzi et al. 2010), high-inclination lines are measured in type 1 objects as well (Mkn 509, MCG-6-30-15; de la Calle Pérez et al. 2010). Moreover, type 1.5 objects invariably exhibit inclination angles lower then 40°, ruling out a simple relation between the inclination of the nuclear obscuring matter (as measured by the optical type) and that of the accreting matter.

Care must be exercised in interpreting direct measurements of the disc inclination through the profile of a relativistically broadened line, though. Measurements of the inclination angles through X-ray spectroscopy in the relativistically blurred line scenario are still affected by large systematic uncertainties. Even in the best studied case (the high-quality "long-look" EPIC spectrum of MCG-6-30-15 taken in 2002) published measurements of the relativistic line profiles by different authors yield values of the disc inclination angle ranging from 20° to 48° (Brenneman & Reynolds 2006, Fabian et al. 2002, Branduardi-Raymont et al. 2001, Reynolds et al. 2004).

3. The quest for the ultimate driver of relativistic effect strength

A number of AGN exhibit relativistically broadened iron lines with an EW ≥300 eV (cf. Sect. 1). Such an extreme strength is difficult to reconcile with theoretical calculations of the EW expected from standard X-ray illuminated relativistic accretion discs (George & Fabian 1991), unless the primary emission illuminating the disc is highly anisotropic. Mechanisms based on strong relativistic effects occurring when the source is located a few gravitational radii from the black hole event horizon have been proposed (Martocchia et al. 2002, Miniutti & Fabian 2004). Indeed, light bending coupled with a variable height of the X-ray primary sources on the disc plane can explain at the same time the extreme strength of relativistic reprocessing spectral components (Fabian et al. 2009, Ponti et al. 2010), and their lack of response to the primary continuum variation (Miniutti & Fabian 2004).

A standard plane-parallel X-ray illuminated accretion disc covering a 2π solid angle should produce an EW∼150 eV for a typical AGN X-ray spectral shape and solar abundances (George & Fabian 1991). However, many of the FERO+GREDOS sources exhibit EWs significantly lower than this. Are there alternatives to explaining this large dynamical range in terms of disk solid angle as seen by the primary source? We will hereby follow a falsification approach to address this problem: we will assume that for "standard" $EW \leq 300$ eV AGN the solid angle is on the average the same, and analyse which consequences this assumption bears on the correlation between EW and other observables.

We first mention the most fundamental limitation of our quest. High-EW reprocessed emission lines can be produced if the disc photosphere is highly ionised (Życki et al. 1994). The data currently do not allow us to test this hypothesis. Fits with a relativistic profile corresponding to being dominated by Fe He-like emission is preferred in 3 out of 11 FERO (de la Calle Pérez et al. 2010), in none of the GREDOS detections. Although in these cases the EW is tendentiously larger then the distribution average (140-230 eV), this parameter space is not exclusively occupied by them. Moreover, there is no correlation between the line

EW and the X-ray luminosity or the accretion rate normalised to the Eddington value. This suggests that disc photoionisation probably does not play a decisive role in determining the strength of relativistic reprocessing for our sample. Much better data quality would be required, however, to resolve the degeneracy between the bulk ionisation state of the line emitting region and other parameters.

Once we neglect the disc ionisation, the EW of a relativistically broadened iron line depends primarily on:

1. the photon index of the illuminating continuum, Γ
2. the disc inclination, $\imath$
3. the iron abundance, Z_{Fe}
4. the "reflection fraction", a parameter which for purely isotropic emission is proportional to the solid angle subtended by the disc at the X-ray source

Approximated formulae for the dependency on the first three parameters are reported by Nandra et al. (2007)[5]. In this Section we will assume initially that the reflection fraction is the same for all objects in the FERO+GREDOS sample and test whether the observed distribution of EW can be reproduced by any of the other three parameters.

Very few measurements of the iron abundance are available in the literature for the objects of our sample. Following the approach after Ballantyne (2010) we have therefore decided to calculate Z_{Fe} using the correlation with the accretion rate in Netzer & Trakhtenbrot (2007).

In Fig. 7 we show the relation between the EW of the relativistically broadened iron line and Γ, $\imath$ and Z for two samples:

1. the full FERO+GREDOS sample (*left panels*)
2. the 12 FERO+GREDOS detections only, once the EW values have been corrected for the dependency of the EW on the other two parameters assuming as common reference the values: Γ_0=1.9; $\imath_0$=30°; $Z_{Fe,0} = Z_{\odot}$.

The EW observed trends against any of the above parameters do not agree with the theoretical predictions. The correlation against the metallicity fails to reproduce the whole dynamical range covered by the EW measurements for $Z_{Fe} \geq 0.5Z_{\odot}$.

Fig. 7 demonstrates that the falsification tests we aimed at fails. We are left with the conclusion that the "reflection fraction" is the main driver of the relativistically broadened iron line EW even when X-ray spectra are not disc-reflection dominated. In Fig. 8 we show the correlation between the EW and the parameter R, which is usually used to characterise quantitatively the reflection fraction. A similar correlation is found between α and R, as expected given the tentative correlation between α and EW shown in Fig. 5. R is proportional to the solid angle, Ω, subtended by the disc at the X-ray isotropic source, and $R = 1$ for $\Omega = 2\pi$. Unfortunately, the scientific payload on-board XMM-newton does not allow the simultaneous measurement of R. We have therefore derived R from literature non-simultaneous measurements. In most cases we have used the results of the BeppoSAX survey of AGN after Dadina 2007, except for those objects for which more recent measurements by *Suzaku* are available: NGC3516 (Markowitz et al. 2008), and IC4329A (Markowitz et al. 2006). With these data, the measured values of R is primarily driven by the strength of the hard ($E \geq 10$ keV) excess above the extrapolation of the primary continuum. These measurements therefore *assume* that the hard X-ray excess is dominated by reflection. In some cases (Turner & Miller 2009, Reeves et al. 2009) it appears that absorption may play a greater role (see also Walton et al. 2010).

Care has to be exercised in interpreting this plot, due to the non-simultaneity of the measurements, as well to the different astrophysical models used to fit the XMM-Newton/EPIC, the *Suzaku* and the BeppoSAX data. Moreover, a contribution to the continuum Compton-reflection certainly comes from optically thick matter at pc-scale, responsible for the bulk of the unresolved component of the narrow K_{α} iron line (Page et al. 2004, Bianchi et al. 2007, Shu et al. 2010). Bearing these caveats in mind, a good agreement between R and EW is found, as already reported by previous authors (Perola et al. 2002, Dadina 2008, Walton et al. 2010). Recently, the possibility that a transmitted component seen through a partial covered absorber could contribute to the emission above 10 keV, which is crucial for the measurement of the reflection fraction, has been suggested in the basis of broadband X-ray measurements (Turner et al. 2009). Studies of sizable samples of bright AGN with missions ensuring a broadband simultaneous coverage such as *Suzaku* or the future Astro-H and*Astrosat* would be very valuable in this respect.

4. Conclusions

In this paper we have tried to address the question: why does the EW of the relativistically broadened K_{α} fluorescent iron line in AGN covers a dynamical range of almost two orders or magnitude if the standard theory (reflection of the X-ray isotropic primary emission by a plane-parallel infinite accretion disc) predicts variations by at most factor of a few?

In a few cases of very strong (EW >300 eV) lines, a "reflection dominated" scenario seems inescapable (Miniutti & Fabian 2004). The advantage of this scenario is that it provides a natural explanation to a wide range of different phenomenologies commonly observed in X-ray bright AGN, such as the "soft excess" (Crummy et al. 2006), and the lack of response of relativistic reprocessed features to changes of the primary illuminating continuum (Miniutti & Fabian 2004, Ponti et al. 2006). Does this scenario hold also for "less extreme", not reflection dominated AGN? Observationally, we confirm that the most likely driver for the variation of the EW is the solid angle subtended by the accretion disc (Fig. 8).

Resonant trapping of fluorescent photons (Matt et al. 1993) can significantly suppress the EW of line emitted by mildly ionised (ξ~a few hundreds erg cm s^{-1}. Alternatively, in many objects of the FERO+GREDOS sample the measured strength of the disk reprocessing features implies a solid angle subtended by the disk $<2\pi$ (assuming isotropic primary emission). What is the ultimate physical driver of the lower-than-standard "reflection fraction" in weak broad-line Seyferts? One possible way to decrease the "effective solid angle" of the reflecting

[5] Although the formula for the dependency of the EW on the spectral index contains a typo. The correct formula is $EW = EW_0 \times [9.66 \times (\Gamma^{-2.80}) - 0.56]$ (Nandra, private communication), where EW_0=144 eV.

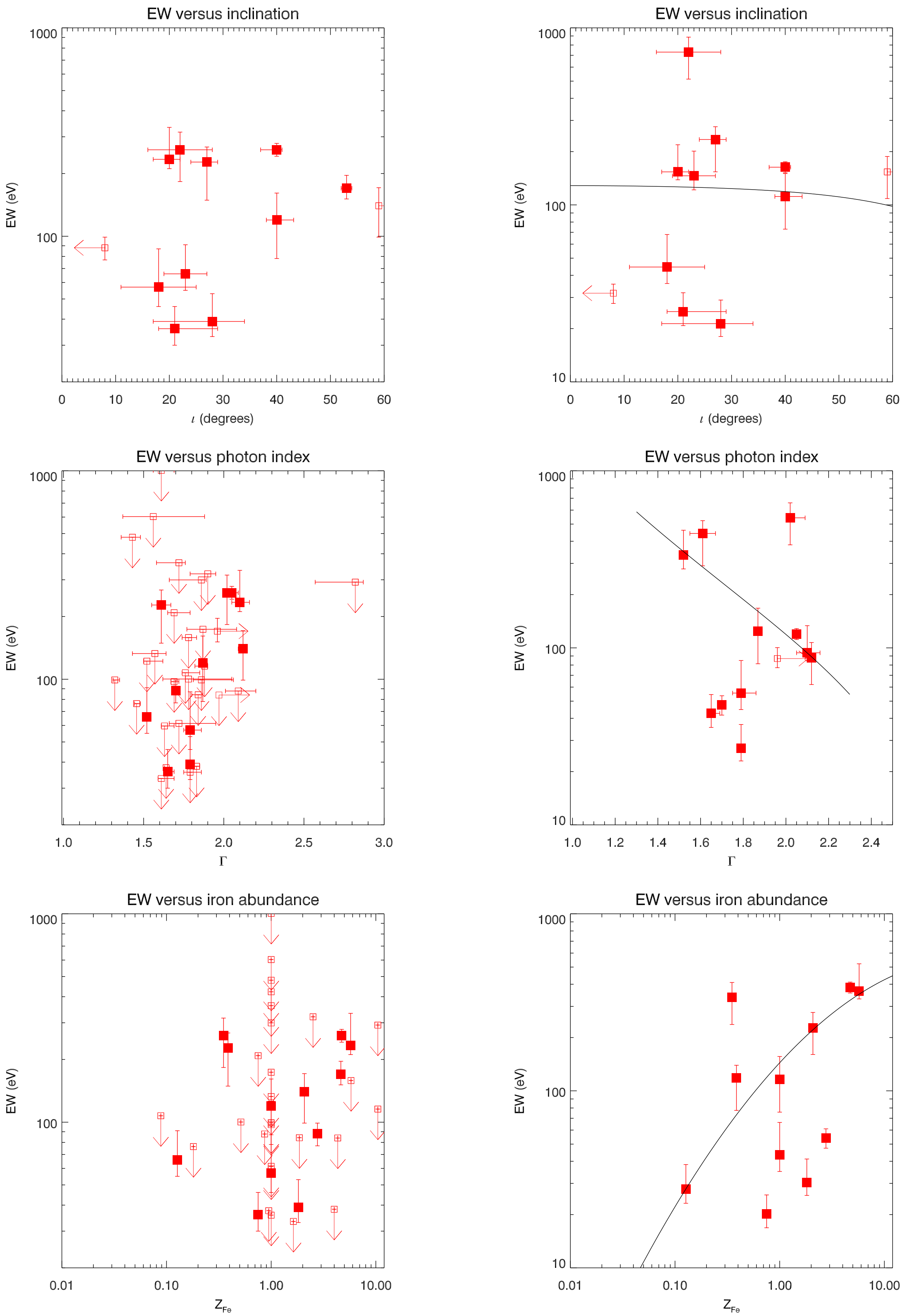

Fig. 7. EW of the relativistically broadened iron line in the FERO+GREDOS sample against the: disc inclination angle (*upper panels*); primary illuminating continuum power-law spectral index (*medium panels*); iron abundance (*lower panels*). The *left column* shows the whole sample, the *right column* shows only the data points corresponding to line detections, once the EW values were corrected for the dependency on the other two parameters according to George & Fabian (1991) and using the following common reference values: Γ_0=1.9; $\imath_0$=30°; $Z_{Fe,0} = Z_{\odot}$. The *solid line* indicates the predicted behaviour according to George & Fabian (1991). *Filled symbols* indicate detections.

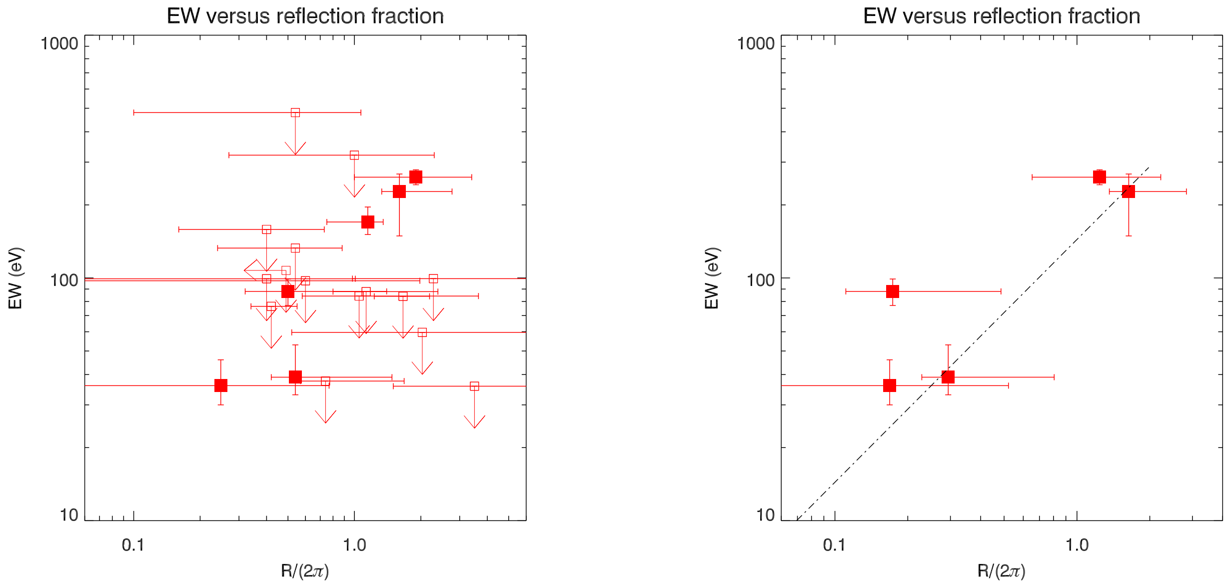

Fig. 8. EW against the "reflection fraction" parameter R in the FERO+GREDOS sample. *Left panel*: all measurements; *Right panel*: detections only, corrected for the EW dependencies on Γ, $\imath$, and Z_{Fe} to the reference values of Fig. 7. The *dashed line* indicates a linear relation, with EW=144 eV for R=1 (George & Fabian 1991).

matter is that the innermost flow is so highly ionised that iron is fully stripped and no fluorescence or recombination lines cannot occur any longer. The ionisation parameter of the disc is expected to increase very rapidly close (and beyond) the ISCO (Reynolds & Fabian 2008), making it quickly "radiatively truncated". The current data are not sensitive to the detailed ionisation state of the relativistic line profiles. Although this prevents a conclusive answer on this possibility, there is no compelling evidence so far for a dependence of the line strength on the rest-frame centroid energy (de la Calle Pérez et al. 2010).

Already at the dawn of X-ray relativistic spectroscopy, Beloborodov (1999) had invoked bulk motion of the primary X-ray continuum emitting plasma away from the accretion disc to explain the weakness of reflection features. Reflection fractions corresponding to $\Omega < \pi$ can be achieved with moderate ($\beta \equiv v/c \simeq 0.3$) bulk velocities, and could be further reduced by scattering of the reflected radiation in an outflowing blob. The X-ray outflowing plasma could be identified with, *e.g.*, the base of a jet, which would at the same time provide a source of the relativistic electrons required for inverse Compton upscattering of disc photons into the X-ray regime.

Alternatively, the disc could be physically truncated in sources with a lower-EW line. This mechanism would also provide a natural explanation to the correlation between the EW and the power-law index of the disc emissivity as a function of radius (Fig. 5). In qualitative terms, a lower EW could be produced by a smaller area of the disc farther away from the black hole, where the relativistic effects are weaker; this would be reflected in the way we fit the data by a low ($\alpha \leq 2$) values. However, an alternative explanation for the same correlation invokes a simpler effect related to the quality of the data: when the red wing of a relativistic line is confused in the underlying continuum, the line profile appears less "relativistic" and at the same time weaker. Therefore an observational bias could also produce the correlation in Fig. 5. Moreover, claims of truncated discs have been made for sources with very different value of accretion rate, from low-luminosity AGN to powerful quasars (Matt et al. 2005, Svoboda et al. 2010, Lobban et al. 2010). This is at odds with a similar scenario invoked to explain the hard/low state in Galactic Black Hole Candidates (GBHCs), typically associated to low accretion states (Fender et al. 2004). A possible way out to reconcile this discrepancy (apart from invoking a different explanation for the lack of relativistic features in high accretion rate AGN) is assuming that powerful quasars never go into the equivalent of the GBHC "low state". States without relativistic spectral features would correspond to the "Very High State" observed, for instance, in the microquasar GRS1915+105 (Fender & Belloni 2004).

The broad iron line could also be produced by localised co-rotating spots on the accretion disc, which illuminate only a small fraction thereof (Pecháček et al. 2005). Indeed, transient redshifted features have been reported in an handful of objects (Turner et al. 2002, Guainazzi 2003) and interpreted in terms of orbiting spots (Dovčiak et al. 2004). Although doubts have been cast on the statistical significance of these effects (Vaughan & Uttley 2008), they have been confirmed by a homogeneous study of a large number of bright sources extracted from the FERO sample (de Marco et al. 2009). The discussion on the reliability of this phenomenology and its relevance for the AGN population as a whole is still open, and will be hopefully settled once more data will be available with future high-throughput missions.

4.1. On alternatives to the relativistic blurring scenarios

Finally, if the spectral complexity in the iron band is due to a completely different mechanism, which does not require general relativistic effects close in the innermost region of the accretion flow (*e.g.*, Turner & Miller 2009), the observations described in this paper cannot be explained in terms of relativistic effects. Turner & Miller

(2009) reviewed recently an alternative scenario where the skewed profile of the K_α iron line is due to partial covering ionised absorption mimicking the broad read wing and the sharp blue drop at $\simeq$7 keV. This scenario delivers statistically equivalent fits to the relativistic reflection scenario for a number of time-averaged X-ray spectra of bright Seyferts (Reeves et al. 2004, Miller et al. 2009), as well as explaining their spectral variability (Miller et al. 2007, 2008, 2010). Readers are referred to Miller (2007) and Turner & Miller (2009) for an exhaustive discussion of strength and weaknesses of both scenarios. Disk winds are predicted theoretically in several configurations of the accretion flow (Proga et al. 2008, Sim et al. 2010), and their impact on the spectral shape above 2 keV cannot be neglected (Reeves et al. 2004). The authors of the current paper are of the opinion the not intuitive geometry that partial covering of the primary X-ray source on scales of a few gravitation radii (Risaliti et al. 2007) requires; and the scale-law between Galactic Black Hole systems (where partial covering surely does not occur) and AGN in the timing-domain (McHardy et al. 2006) are serious shortcomings of the "partial covering" scenario. In this context, the possible discovery of "clean AGN" (*i.e.*, AGN whose X-ray soft X-ray spectrum does not show evidence for a warm absorber; Emmanoulopoulos et al. 2011) are a potentially crucial testbed for the robustness of Fe K_α broad line detections.

Turner & Miller (2009) - and many papers referenced therein - discuss these shortcomings. They stress that the light bending scenario - introduced to explain an unexpected lack of correlation between the short-term variability of the primary continuum and the disk reflection features - also requires rather "ad hoc" assumptions on the X-ray source geometry and dynamics. The source has to be compact, and moving in a vertical direction on short time-scales while maintaining its stability. While the base of a jet could in principle provide a physical location for this compact, highly dynamical source of high-energy photons, some of the difficulties of this picture have been recently discussed by Życki et al. (2010). In the partial covering scenario the physical scaling of the accreting system with mass and luminosity implies a scaling of the clumpy covering material with mass. While short-time variations at high-energy are still most likely due to intrinsic fluctuations of the source, the spectral curvature below the Fe K_α line and its variation on long-timescales are successfully modelled with clumpy material in a disk wind.

It remains highly controversial which falsification experiment(s) could eventually settle the issues. General consensus exists that studies of large AGN X-ray high-quality broad-band spectral samples with operational (*Suzaku*; see, *e.g.*, the recent work by Patrick et al., 2010) or future (Astro-H,*Astrosat*, IXO) missions will be crucial. A statistical comparison of the fit quality produced by different scenarios on the same sample, as well as of the corresponding observable distributions, would be a valuable exercise. This paper, the last of a series of studies inspired by the goal of putting the discussion on relativistic X-ray spectroscopy on a sound statistical basis, aims at giving a contribution to this ongoing effort.

Table 4. Summary of spectral fit results for the GREDOS sample: relativistic line. All measurements refer to a rest frame centroid energy E_c = 6.4 keV. Upper limits are at the 90% level.

Source	$\imath$ (°)	α	EW (eV)
NGC4507	...	...	<130
Mrk348	...	...	<300
NGC4388	...	...	...[a]
Mrk6	...	...	<480
NGC2110	...	...	<100
NGC5252	...	...	<600
NGC7172	...	...	<60
1ES0241+622	...	...	<1000
GRS1734-292	...	...	<420
NGC5506	$40.0\pm^{3.1}_{1.9}$	$1.88\pm^{0.16}_{0.23}$	120 ± 40
NGC4151	...	...	<80
NGC526	...	...	<250
MCG-05-23-016	$38\pm^{7}_{5}$	$1.41^{0.04}_{0.30}$	55 ± 26

[a]unconstrained

Appendix A. Spectral results on the GREDOS sample

Tab. 3 summarises the results for the continuum components. In Tab. 4 we report the results on the relativistic line profiles. For non-detected lines we report only the 90% upper limit on the Equivalent Width for a fixed $E_c \equiv 6.4$ keV. The parameters refers to a value of the spin corresponding to a maximally spinning black hole ($a = 0.998$). In all cases, a solution corresponding to a neutral emitting gas (E_c=6.4 keV) is preferred. A gallery of spectra and best-fit model is shown in Fig. 9, whereas the line profiles (only for detections) are shown in Fig. 2. These line profiles are obtained from the data/model ratio against the best-fit model once the relativistic line profile (`kyrline` component in the best-fit model) is removed. In a few cases the strength of the continuum reflection as measured by EPIC is inconsistent with the broad iron line EW, or lack thereof. We stress that fits of the EPIC-pn spectra are relatively insensitive to the exact value of the reflection fraction, which is primarily driven by the depth and shape of the iron photo-absorption edge. This feature is degenerate with the photo-absorption column density in fits of obscured AGN over an energy band limited to 10 keV. One should therefore refrain from over-interpreting the astrophysical implications of these results.

Acknowledgements. Based on observations obtained with XMM-Newton, an ESA science mission with instruments and contributions directly funded by ESA Member States and NASA. This research has made use of the NASA/IPAC Extragalactic Database (NED) which is operated by the Jet Propulsion Laboratory, California Institute of Technology, under contract with the National Aeronautics and Space Administration. The authors thank G.Cusumano, V.La Parola and G.Miniutti for comments on an early version of the manuscript. Constructive comments by the referee, Lance Miller, substantially improved the quality of the paper, allowing us to present our results in a more balanced and unbiased way.

References

Agol E., Krolik J.H., 2000, ApJ, 528, 161
Anders E. & Grevesse N., 1989, Geochimica et Cosmochimica Acta 53, 197
Antonucci R., 1993, ARA&A 31, 473
Awaki H., Koyama K., Inoue H., Halpern J.O., 1991, PASJ 43, 195
Ballantyne D.R., 2010, ApJ, 708, L1

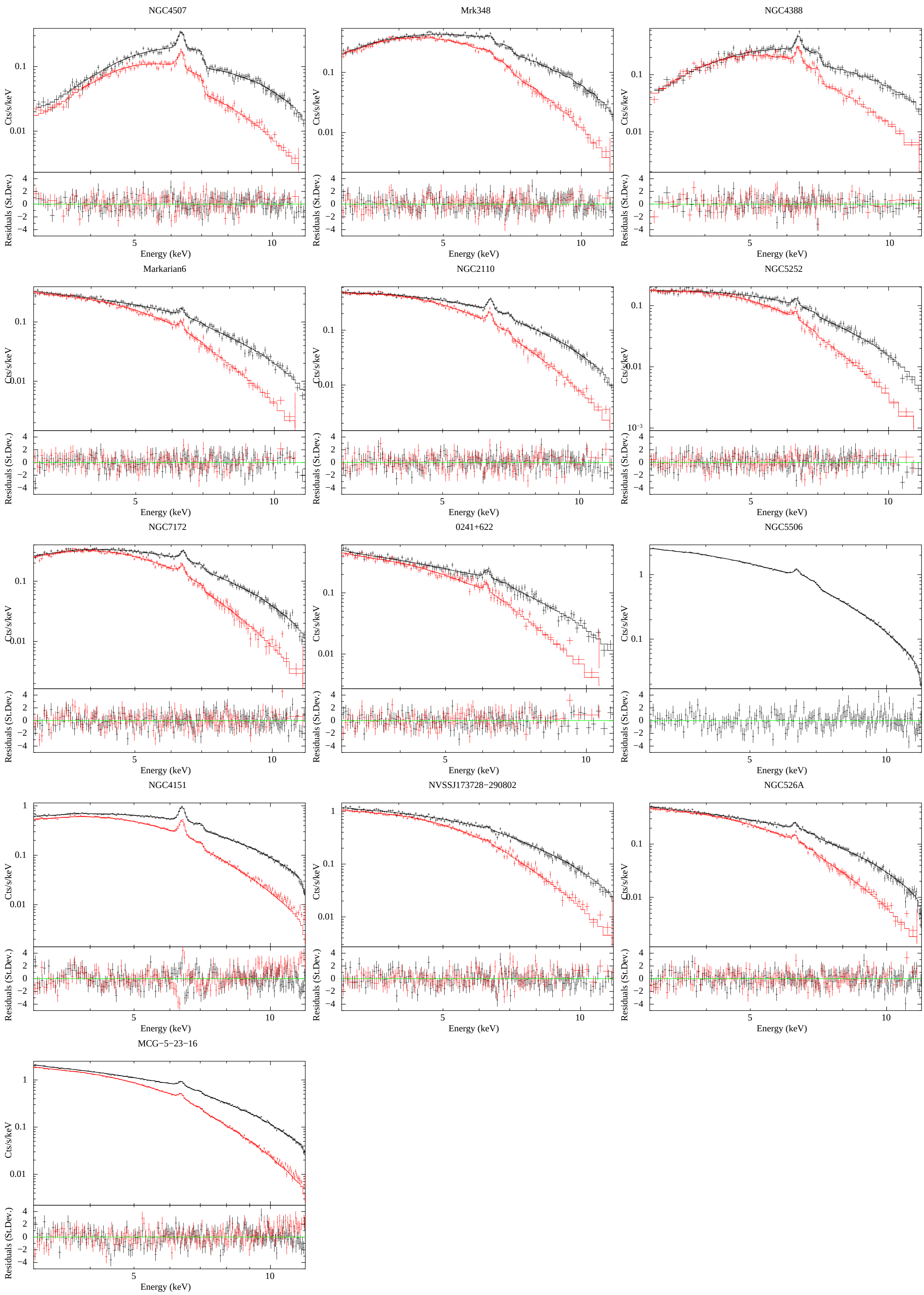

Fig. 9. Spectra (*upper panels*) and residuals in units of standard deviations (*lower panels*) when the best-fit models as in Tab. 3 are applied to the GREDOS sample.

Table 3. Summary of spectral fit results for the GREDOS sample: continuum components

Source	Γ	$N_{H,1}$ (10^{22} cm^{-2})	$N_{H,2}$ (10^{22} cm^{-2})	$\log(\xi)/{C_f}^a$	${R_{nr}}^b$	${R_r}^c$	Abs.Model^d
NGC4507	$1.57\pm^{0.07}_{0.14}$	$58\pm^{41}_{5}d$	7 ± 3	<2.1	$0.55\pm^{0.14}_{0.06}$	<0.1	CW
NGC4388	$1.86\pm^{0.03}_{0.35}$	$21.2\pm^{0.9}_{0.5}$	4 ± 3	$2.0\pm^{0.7}_{0.2}$	0.8 ± 0.3	$0.26\pm^{0.42}_{0.06}$	CW
Mrk6	$1.43\pm^{0.05}_{0.07}$	$1.57\pm^{0.13}_{0.12}$	...	0.85 ± 0.02	<0.4	<2.9	PC
NGC2110	$1.69\pm^{0.03}_{0.02}$	$2.89\pm^{0.12}_{0.36}$	$9.3\pm^{1.0}_{2.1}$	...	0.9 ± 0.5	3.4 ± 0.7	DC
NGC5252	$1.56\pm^{0.32}_{0.19}$	$3.5\pm^{0.9}_{1.3}$	$16\pm^{25}_{2}$	...	<0.1	0.4	DC
NGC7172	$1.63\pm^{0.06}_{0.02}$	13.3 ± 0.2	...	...	<0.1	$0.68\pm^{0.10}_{0.03}$	SC
1ES0241+622	$1.61\pm^{0.09}_{0.04}$	$0.46\pm^{0.07}_{0.04}$	...	...	<0.6	<0.1	SC
GRS1734-292	$1.41\pm^{0.03}_{0.02}$	1.41 ± 0.02	...	...	<0.1	<0.4	SC
NGC5506	$1.689\pm^{0.011}_{0.013}$	$3.4\pm^{0.7}_{0.5}$	$1.5\pm^{0.5}_{0.8}$	<-0.27	<0.1	<0.1	CW
NGC4151	$1.446\pm^{0.010}_{0.009}$	$13.21\pm^{0.14}_{0.25}$	...	0.853 ± 0.004	$1.07\pm^{0.09}_{0.56}$	<0.1	PC
NGC526	$1.457\pm^{0.021}_{0.013}$	$1.56\pm^{0.04}_{0.03}$	...	...	<0.06	<0.12	SC
MCG-05-23-016	$1.632\pm^{0.010}_{0.016}$	$1.849\pm^{0.014}_{0.040}$	...	...	<0.64	<0.10	SC

[a]ionisation parameter for the warm absorber component for model CW or covering fraction of the patchy absorber for model PC
[b]ratio between the normalisation of the non-relativistic reflection component and the primary power-law
[c]ratio between the normalisation of the relativistic reflection component and the primary power-law
[d]Absorption model. Legenda: SC = single cold absorber; DC = double cold absorber; PC = partial covering; CW = cold and warm absorber

Beckmann V., Gehrels N., Favre P., et al., 2004, ApJ, 614, 641
Beloborodov A.M., 1999, ApJ, 510, L123
Bennett C.L., et al., 2003, ApJS, 148, 1
Bianchi S., Matt G., 2002, A&A, 387, 76
Bianchi S., Guainazzi M., Chiaberge M., 2006, A&A, 448, 499
Bianchi S., Guainazzi M., Matt G., Fonseca-Bonilla N., 2007, A&A, 467, L19
Bianchi S., de Angelis I., Matt G., et al., submitted to A&A
Branduardi-Raymont G., Sako M., Kahn S.M., Brinkman A.S., Kaastra J.S., Page M.J., 2001, A&A, 365, L140
Brenneman L.W., Reynolds C.S., 2006, ApJ, 652, 1028
Chartas G., Eracleous M., Dai X., Agol E., Gallagher S., 2007, ApJ, 661, 678
Crummy J., Fabian A.C., Gallo L., Ross R.R., 2006, MNRAS, 365, 1067
Cusumano G., La Parola V., Segreto A., et al., 2010, A&A, 510, 48
Dadina M., 2007, A&A, 461, 1209
Dadina M., 2008, A&A, 485, 417
Dadina M., Guainazzi M., Cappi M., et al., 2010, A&A, 516, A9
de la Calle Pérez I., Longinotti A., Guainazzi M., et al., 2010, A&A, submitted
Della Ceca R., Ballo L., Braito V., Maccacaro T., 2005, ApJ, 627, 706
de Marco B., Iwasawa K., Cappi M., et al., 2009, A&A, 507, 159
Dewangan G.C., Griffiths R.E., Schurch N.E., 2003, ApJ, 592, 52
Dovčiak M., Bianchi S., Guainazzi M., Karas V., Matt G., 2004, MNRAS, 350, 745
Emmanoulopoulos D., Papadakis I.E., McHardy I.M., Nicastro F., Bianchi S., Arevalo P., 2011, MNRAS, in press (arXiv:1104.0044)
Fabian A.C., Iwasawa K., Reynolds C.S., Young A.J., 2000, PASP, 112, 1145]
Fabian A.C., Rees M.J., Stella L., White N.E., 1989, MNRAS, 238, 729
Fabian A.C. & Vaughan S., 2003, MNRAS, 340, L28
Fabian A.C., Vaughan S., Nandra K., et al., 2002, MNRAS, 335, L1
Fabian A.C., Zoghbi A., Ross R.R., et al., 2009, Nat, 459, 540
Fender R.P., Belloni T.M., 2004, ARA&A, 42, 317
Fender R.P., Belloni T.M., Gallo E., 2004, MNRAS, 355, 1105
Ferland G. J., Korista K.T., Verner D.A., Ferguson J.W., Kingdon J.B., Verner E.M., 1998, PASP, 110, 761
Gabriel C., Denby M., Fyfe D. J., Hoar J., Ibarra A., 2003, in ASP Conf. Ser., Vol. 314 Astronomical Data Analysis Software and Systems XIII, eds. F. Ochsenbein, M. Allen, & D. Egret (San Francisco: ASP), 759
George I.M., Fabian A.C., 1991, MNRAS, 249, 352
Guainazzi M., 2003, A&A, 401, 903
Guainazzi M., Bianchi S., Dovĉiak M., 2006, AN, 327, 1032
Guainazzi M., Risaliti G., Nucita A., et al., 2009, A&A, 505, 589
Guainazzi M., Bianchi S., Matt G., Dadina M., Kaastra J., Malzac J., Risaliti G., 2010, MNRAS, 406, 2013
Isobe T., Feigelson E.D., Nelson P.I., 1986, ApJ, 306, 490
Krolik J.H, Hawley J.F., 2002, ApJ, 573, 754
Krumpe M., Lamer G., Schwope A., Husemann B., 2007, A&A, 470, 497
Lampton M., Margon B., Bowyer S., 1976, ApJ, 207, 894
Laor A, 1991, ApJ, 376, 90
Lobban A.P., Reeves J.N., Porquet D., et al., 2010, MNRAS, 408, 551
Longinotti A.L., Cappi M., Nandra K., Dadina M., Pellegrini S., 2003, A&A, 410, 471
Longinotti A.L., Bianchi S., Santos LLeo M., et al., 2007, MNRAS, 374, 237
Magdziarz P.& Zdziarski A.A., 1995, MNRAS 273, 837
Markowitz A., Reeves J.N., Braito V., 2006, ApJ, 646, 783
Markowitz A., Reeves J.N., Miniutti G., et al., PASJ, 60, 277
Martocchia A., Matt G., Karas V., 2002, 383, L23
Mason K., et al., 2003, ApJ, 582, 95
Matt G., 2002, MNRAS, 337 147
Matt G., Bianchi S., d'Ammando F., Martocchia A., A&A, 421, 473
Matt G., Fabian A.C., Ross R.R., 1993, MNRAS 261, 346
Matt G., Perola G.C., Piro L., Stella L., 1992, A&A, 257, 63 (erratum: 263, 453)
Matt G., Porquet D., Bianchi S., et al., A&A, 435, 857
McHardy I., Koerding E., Knigge C., Uttley P., Fender R.P., 2006, Nat, 444, 730
Miller J.M., 2007, ARA&A, 45, 441
Miller L., Turner T.J., Reeves J., 2008, A&A, 483, 437
Miller L., Turner T.J., Reeves J., 2009, MNRAS, 399, L69
Miller L., Turner T.J., Reeves J.N., George I.M., Kraemer S.B., Wingert B., 2007, A&A, 463, 131
Miller L., Turner T.J., 2010, MNRAS, in press (astro-ph 1006.5035)
Miller L., Turner T.J., Reeves J.N., Lobban A., Kraemer S.B., Crenshaw D.M., 2010, MNRAS, 403, 196
Miniutti G., Fabian A.C., 2004, MNRAS, 349, 1435
Nandra K., George I.M., Mushotzky R.F., Turner T.J., Yaqoob T., 1997, ApJ 467, 70
Nandra K., O'Neill P.M., George I.M., Reeves J.N., 2007, MNRAS, 382, 194
Nandra K., Pounds K.A., 1994, MNRAS, 268, 405
Nayakshin S., Kazanas D., Kallman T.R., 2000, ApJ, 537, 833
Netzer H., Trakhtenbrot B., 2007, ApJ, 654, 754
Netzer H., Turner T.J., George I.M., 1998, ApJ, 504, 680
Page K.L., O'Brien P.T., Reeves J.N., Turner M.J.L., 2004, MNRAS, 347, 316
Patrick A.R., Reeves J.N., Porquet D., Markowitz A.G., Lobban A.P., Terashima Y., 2010, MNRAS, in press (arXiv:1010.2080)
Pecháček T., Dovčiak M., Karas V., Matt G., 2005, A&A, 441, 855
Perola G.C., Matt G., Cappi M., Fiore F., Guainazzi M., Maraschi L., Petrucci P., Piro L. et al., 2002, A&A, 389, 202
Piconcelli E., Sánchez Portal M., Guainazzi M., et al., A&A, 453, 839
Ponti G., Fabian A.C., Gallo L.C., et al. , 2010, MNRAS, 406, 2591
Ponti G., Miniutti G., Cappi M., Maraschi L., Fabian A.C., Iwasawa K., 2006, MNRAS, 368, 903
Porquet D., 2006, A&A, 445, L5

Pounds K.A., Nandra K., Stewart G.C., George I.M., Fabian A.C., 1990, Nat, 344, 132
Proga D., Ostriker J.P., Kurosawa R., 2008, ApJ, 676, 101
Reeves J.N., Awaki H., Dewangan G.C., et al., 2007, PASJ, 59, 301
Reeves J.N., Nandra K., George I.M., Pounds K., Turner T.J., Yaqoob T., 2004, ApJ, 602, 648
Reeves J.N., O'Brien P., Braito V., et al., 2009, ApJ, 701, 493
Reynolds C.S., Fabian A.C., 2008, ApJ, 675, 1048
Reynolds C.S., Novak M.A., 2003, Ph.R. 377, 389
Reynolds C.S., Wilms J., Begelman M.C., Staubert R., Kendziorra E., 2004, 349, MNRAS, 1153
Revnivtsev M., et al., 2004, A&A, 418, 927
Risaliti G., 2002, A&A, 386, 379
Risaliti G., Elvis M., Fabbiano G., Baldi A., Zezas A., Salvati M., 2007, ApJ, 659, L111
Risaliti G., Miniutti G., Elvis M., et al., 2009, ApJ, 696, 160
Ross R.R., Fabian A.C., 2005, MNRAS, 358, 211
Schmitt J.H.M.M., 1985, A&A, 293, 178
Schurch N.J., Griffiths R.E, Warwick R.S., 2006, MNRAS, 317, 211
Schurch N.J., Warwick R.S., Griffiths R.E., Sembay S., 2003, MNRAS, 345, 423
Shu X.W., Yaqoob T., Wang J.X., ApJS, 187, 581
Sim S.A, Proga D., Miller L., Long K.S., Turner T.J., 2010, MNRAS, 408, 1386
Strüder L., Briel U., Dannerl K., et al., 2001, A&A 365, L18
Svoboda J., Guainazzi M., Karas V., 2010, A&A, 512, 62
Tanaka Y., Nandra K., Fabian A.C., et al., 1995, Nat, 375, 659
Turner M.J.L., Abbey A., Arnaud M., et al., 2001, A&A 365, L27
Turner T.J., George I.M., Nandra K., Mushotzky R.F., 1997, ApJS 113, 23
Turner T.J., Miller L., 2009, A&ARv, 17, 47
Turner T.J., Miller L., Kraemer S.B., Reeves J.N., Pounds K.A, 2009, ApJ, 698, 99
Turner T.J., Mushotzky R.F., Yaqoob T., et al., 2002, ApJ, 574, L12
Vaughan S., Uttley P., 2008, MNRAS, 390, 412
Véron-Cetty M.-P., Véron P., 2010, 518, 10
Vignali C., Piconcelli E., Bianchi S., Miniutti G., 2008, MNRAS, 388, 761
Walton D.J., Reis R.C., Fabian A.C, 2010, MNRAS, 408, 601
Wilms J., Reynolds C.S., Begelman M.C., et al., 2001, MNRAS, 328, L27
Życki P., Krolik J.H., Zdziarski A.A., Kallman T.R., 1994, ApJ, 437, 596
Życki P., Ebisawa K., Niedźwiecki A., Miyakawa T., 2010, PASJ, 62, 1185